Chapter 3

Artefacts and Deconvolution

Using a simple computer simulation for AFM imaging in the contact mode, the convolution effect is demonstrated in the atomic scale. Artefacts having the size of the effective tip are reported. The convolution effect occurs also in larger scales resulting in an effective broadening of sample's features. We discuss the conditions under which one can obtain true topographical information. An experimental procedure for determining the tip's radius of curvature is described. It is shown that avoiding normal deformations (low loads) and for known tip radii the features of the sample can be approximately recovered.

3.1 Atomic Scale Artefacts. Simple Computer Simulations

Even though Atomic Force Microscopy (AFM) [1, 2] has been successful in imaging surfaces with atomic resolution, it is still doubtful whether true atomic resolution is really obtained. Most images reported show perfect crystal lattices or defects much larger than atomic scale defects. On the other hand, the situation in Scanning Tunneling Microscopy (STM) is quite different and images with point defects are routinely obtained [3]. This is usually attributed to the fact that the tunneling current is laterally localized in an area of few Ångstroms in diameter, while in force microscopy the effective part of the probing tip is laterally much larger. Thus the atomic resolution is not obtained by a point interaction but by a superposition (convolution) of several interactions between the atoms in the tip and the sample.

This assumption is justifiable if one considers that even in the case of a diamond tip and a diamond sample, using typical loads, the tip-sample contact area is larger than a single-atom one [4, 5]. The two surfaces (tip and sample) are generally deformed when they are in contact [6]. For softer materials this tendency for larger contact areas under load is even more prevalent [4]. For materials with layered structures (e.g. pyrolytic graphite) the assumption that the tip drags a flake of the material as it scans the surface has proved to be very fruitful [7, 8] and provides results in agreement with the experiments.

Especially for the layered materials the same considerations of flake-like tips (or multiple-atom tips) can be also applied to the STM imaging mechanism [7, 9, 10]. However, the usual case in STM pictures is the imaging of single-point defects in a variety of materials. This fact excludes the possibility of laterally large effective tips as has been shown [11].

Thus, there are two physical mechanisms that make the tip-sample contact area become of some considerable size: a) loads (even the most low ones) result in a flat contact area of considerable size, b) especially for layered materials the tip drags a flake of the sample probed and this flake is the effective tip. The main difference between the two cases is that while in the first case the material of the tip is in general different from the material of the sample, in the second case the effective flake like tip is of the same material.

In this study simple computer simulations are performed imaging a point defect in the perspective of demonstrating situations in which the periodicity of the lattice is reproduced without probing the atomistic details of the sample (false atomic resolution) or alternatively, cases in which individual atoms and defects are imaged (true atomic resolution).

The sample used is a fcc surface consisting of two (111) planes. The forces between the tip and the surface are calculated by adding the pair interactions between the tip atoms and each atom in the sample which are modelled by a pairwise Lennard-Jones potential:

$$U_w(r) \;=\; 4\epsilon_w \left((\frac{\sigma_w}{r})^{12} \;-\; (\frac{\sigma_w}{r})^{6} \right) \tag{3.1}$$

The point defect used is a vacancy in the upper layer of the fcc lattice. Thermal motion and surface relaxation are not implemented since they do not substantially affect the images obtained when introduced. Furthermore the point defect could also be a contaminant atom and in this case the relaxation of the surface would be quite different. The present study is of qualitative nature and not material specific and we are only interested in the general features of the images. Two modes of AFM operation are simulated: constant height and constant force (in the contact regime). In both cases the images obtained have the same qualitative features.

A number of different pyramid-like tips ending in one atom have been used revealing, as expected due to the steepness of the L-J potential in the repulsive regime, that it is sufficient to consider only the end atom of the tip. Consequently in further simulations only one close- packed layer of atoms is used as a flake-like tip. The lattice constants of the tip are taken to be identical to those of the sample.

Using a single-atom tip every individual site in the surface is imaged (fig. 3.1(left)). Thus a monoatomic probe is apparently capable of imaging with true atomic resolution. On the other hand, using even a rather small flake-like tip consisting of 7 atoms and in registry with the sample, an imaginary atom is present in the position of the vacancy as can be clearly seen in fig. 3.1(right). The vacancy has disappeared due to the coherent superposition of the forces between all the tip atoms and each one in the sample. The crystal lattice seems to be perfect although this is not really the case (false atomic resolution). In addition, it is worth mentioning that the flake-like tip is depicted in the

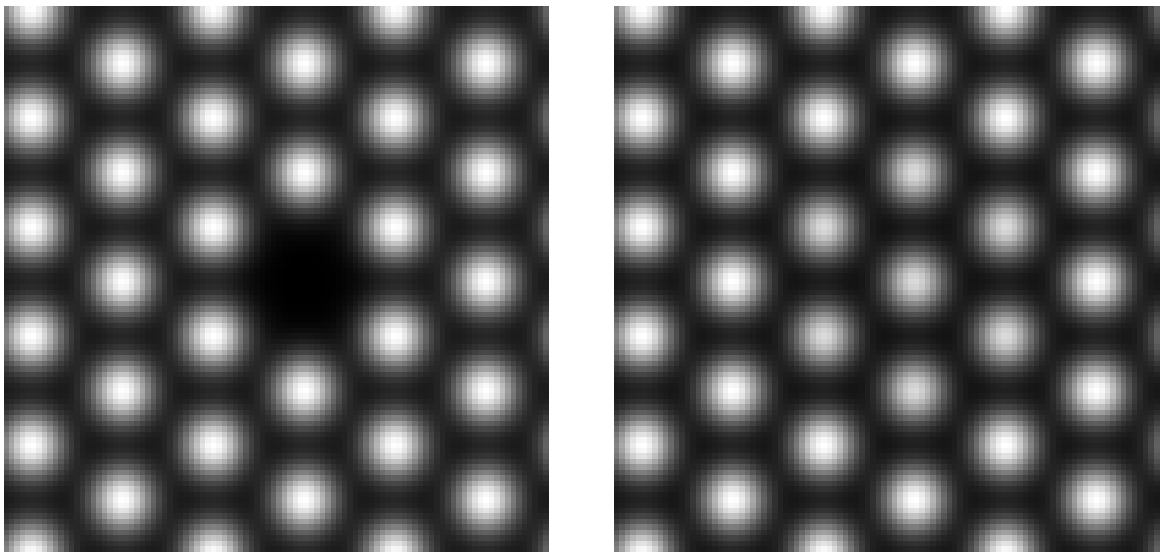

Figure 3.1: *AFM images of a fcc lattice with an atomic vacancy. (left) When the scanning is carried out with a single-atom tip the vacancy is clearly imaged. (right) When the same surface is scanned by a 7-atom flake-like tip, having its atoms in registry with the atoms of the lattice, the vacancy disappears and an imaginary atom is imaged instead.*

picture by the seven atoms of the sample (the imaginary one and those surrounding it) being more vaguely imaged. Thus a fingerprint of the tip can be observed on the scanning image. can be observed on the scanning image. If the tip is rotated and consequently the tip-atoms are placed out of registry with respect to the surface atoms, the image will be distorted due to the incoherent superposition of the interactions. In fig. 3.2(left) the 7-atom tip is rotated by 14^o and the lattice still looks pretty regular. However, in fig. 3.2(right) the tip is rotated by 22.5^o and the distortion around the point vacancy is much stronger, giving the impression of an extended defect. Further away from the distortion, areas with a periodical pattern are observed in agreement with experimental and simulation findings [8, 2]. In order to further emphasize the effect of the tip size a series of simulations is performed using a 31-atom tip. Since the tip now consists of more atoms the forces are considerably larger and the crystal lattice looks completely regular when the tip is in registry as is evident in fig. 3.3(right). In fig. 3.3(left) the same area of the sample is scanned by a single-atom tip for comparison. When the tip is out of registry the distortion becomes much larger revealing the size of the effective tip. As is shown in fig. 3.4(left) a rotation of 14^o has a relatively weak effect but by rotating the tip 2.5^o more a strong distortion is created (fig. 3.4(right)). This kind of distortions could be interpreted wrongly as large monolayer-deep depressions. However, it is a tip artifact produced by the *single* vacancy in the lattice.

The model system that has been considered is closer to layered materials since the flake tips used have the same lattice constants as the sample probed. Nevertheless, as has

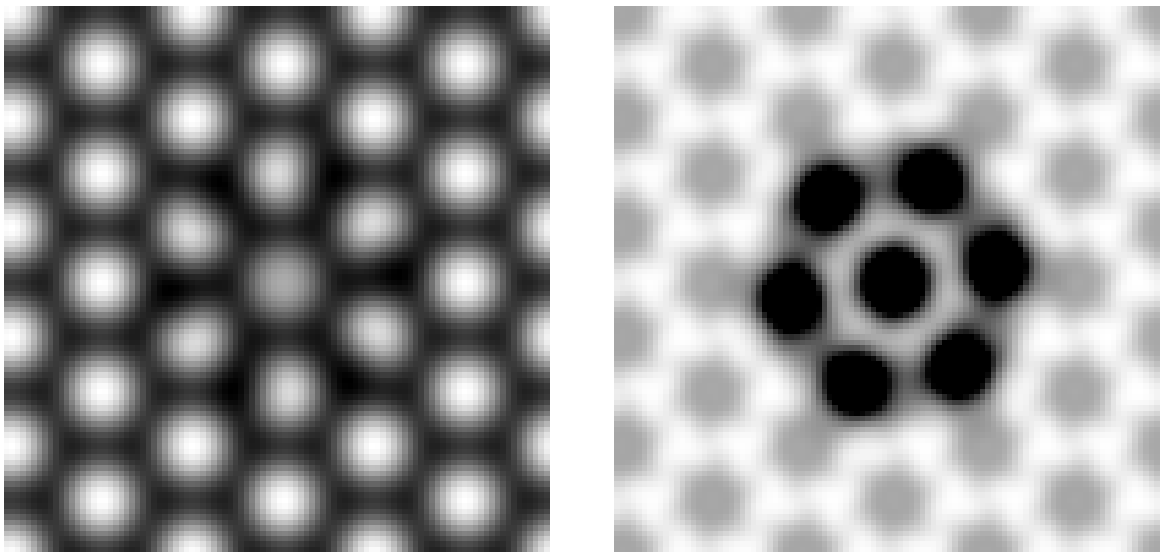

Figure 3.2: *AFM images scanned by the 7-atom flake-like tip out of registry. The distortion of the images due to incoherent superposition is of the scale of the dimensions of the flake. (left) The orientation angle is* 14^o *resulting in a relatively weak distortion. (right) The orientation angle is* 22.5^o *and a strong artifact is created.*

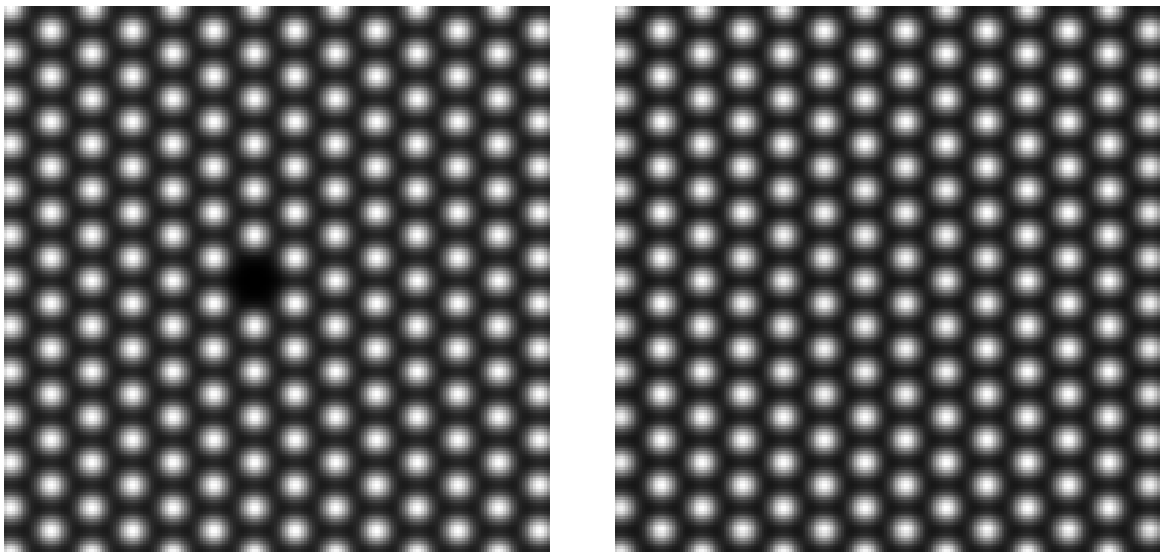

Figure 3.3: *The scanning covers a larger area of the sample. (left) The scanning has been performed using a single-atom tip. (right) A 31-atom flake-like tip is used in registry with the sample resulting in an image with a perfect periodicity and the vacancy has disappeared.*

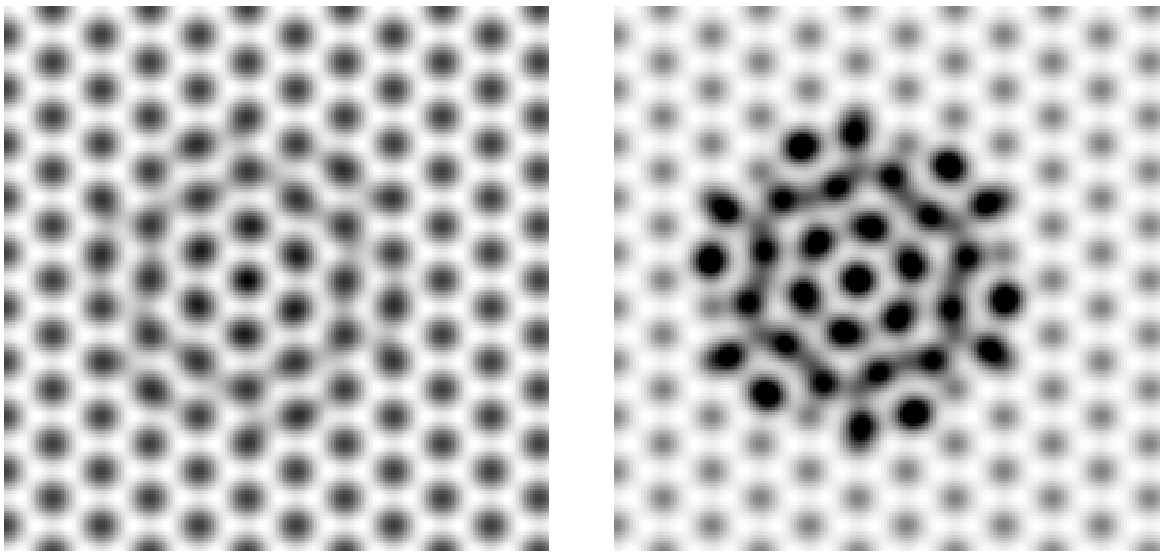

Figure 3.4: *AFM images using the 31-atom flake-like tip out of registry. The distortion of the images is again of the scale of the dimensions of the flake. (left) The orientation angle is* 14^o *and the distortion is relatively weak. (right) The orientation angle is* 17.5^o*. Due to the incoherent convolution a strong artifact is created. This kind of tip-artifacts can be mistaken for large monolayer-deep depressions.*

been stated even for hard materials the contact area is deformed and flattened, thus, the situation can be treated as if the contact area is a flake. The "flake" regarded now has in general different lattice constants making the situation more complicated and material specific (as far as the lattice constants are concerned). However, for the sample of one vacancy considered here, the qualitative features of the images remain the same and furthermore the artefacts generated are expected in general to be more intense.

As can be clearly deduced from the simple demonstration above true atomic resolution can be obtained if the effective tip is a single atom. An elegant experimental demonstration of this fact has appeared recently [12]. Furthermore, one should be very careful in interpreting AFM images since even a one point-defect can generate tip artifacts of the size of the effective tip on the nanometer scale. This effect has been actually observed on larger scales not due to vacancies but due to sharp points (protrusions) in a lattice [13]. Fig. 3.1(right) and 3.3(right) demonstrate clearly why point-defects in layered materials are not observed. The tip carries a piece (sliding plane) of the material in registry with the surface and the image is obtained due to coherent superposition of forces between the atoms in the sliding plane and the sample atoms. Thus, an imaginary atom appears in the vacancy and the periodicity of the layered crystal is reproduced fully but falsely.

If the sliding plane is out of registry with respect to the sample, a single point defect is capable of generating tip artifacts having the size of the effective tip and giving the impression of rather large deformed or contaminated areas. Outside the artifact generated

by the vacancy the atoms look more elongated and even multiple. This is due to the registry mismatch. The images are distorted as if they were generated by a multiple tip.

3.2 Artefacts at the Scale of Tip Radius

For topographic SFM studies of larger scale structures the macroscopic shape of the tip also becomes important. A tip with a relatively large cone angle fails to penetrate into deep and narrow grooves on the sample surface. This leads to underestimation of their depth and smoothing of their edges (fig. 3.5a). Although the height of protrusions can be recorded quite accurately their edges are being smoothed and their lateral size is overestimated (fig. 3.5b).

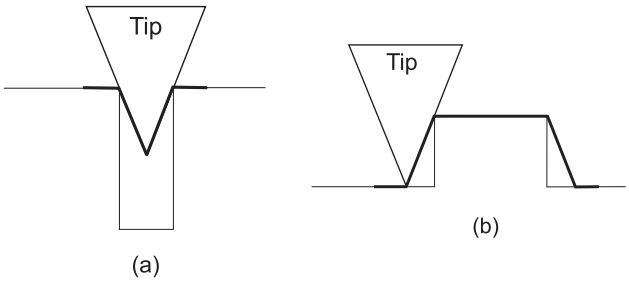

Figure 3.5: *Effect of tip geometry on imaging (thick line) a) a groove and b) a protrusion. Due to finite size of the tip artefacts are prodruced and the resulting image is a convolution between the shape of the tip and the topography of the sample.*

The apparent sizes of features can be also affected by the topography around them. For example, if one investigates particles adsorbed on a rough substrate their shape will be partially determined by the topography of the substrate around them. Fig. 3.6 shows schematically this distortion: Even if two particles are exactly the same, they will be imaged differently if one is on a peak and the other in a valley, due to convolution of the tip and the sample.

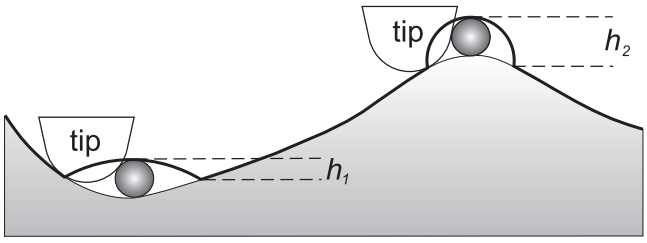

Figure 3.6: *Schematic drawing demonstrating the dependence of the particle shape on the finite tip radius and the local topography of the substrate. The thick line shows the apparent height corrugation. The particle in the valley seems lower and more flattened than the particle on the peak ($h_1 < h_2$).*

3.3 Measuring Feature Heights

A constant normal-force image represents correctly the topography of the sample only if the cantilever spring constant is much weaker than the tip-sample interaction stiffness and the set-point force is chosen to be low [14] . Otherwise, for the same applied load, a compliant part of the sample will be indented more by the tip than a rigid one. Hence, the indentation depth will change during scanning.

We can investigate the magnitude of this effect by calculations based on contact mechanics. The reduced elastic modulus K for the tip-sample system can be written in terms of the Poisson ratio ν and the Young's modulus E of the tip and the sample

$$\frac{1}{K} = \frac{3}{4}[(\frac{1-\nu_{tip}^2}{E_{tip}}) + (\frac{1-\nu_{sample}^2}{E_{sample}})] \tag{3.2}$$

The applied loads are usually low in SFM; hence, the adhesive forces have to be taken into account and the non-adhesive contact theory of Hertz [15] cannot be applied. There are two theories for adhesive contact: (1) JKRS [16] where the two adhering solids stick together, forming a connecting neck, when in contact and DMT [17] where the attractive forces acting outside the region of contact give an effective additional load in the Hertz equations. Maugis et al. [18] has recently developed a model where JKRS and DMT are opposite ends of a spectrum of a non-dimensional parameter:

$$\lambda = \frac{2.06}{z_0}(\frac{w^2 R}{\pi K^2})^{1/3} \tag{3.3}$$

Here, w is the Dupré adhesion energy, z_0 is the equilibrium interatomic distance and $1/R = 1/R_{tip} + 1/R_{sample}$ the tip-sample reduced curvature.

For values of λ in the range of 1 or greater JKRS is a good approximation, while for $\lambda \leq 0.3$ DMT should be used. The adhesion energy can be evaluated by the pull-off force $P_s = n\pi Rw$ ($n \approx 1.5-2$) taken by F-d curves. For a typical tip $-$ PS globule combination: $\nu_{tip} = 0.27$ [19], $E_{tip} = 130 - 150$ GPa [20, 21], $\nu_{sample} = 0.33$ [22], $E_{sample} = 4$ GPa [22], $R_{sample} = 10$ nm, $P_s = 2$ nN. λ was calculated to be close to 1 and subsequently JKRS theory can be used. The penetration depth δ for an applied load P is

$$\delta = \frac{\alpha^2}{R} - (\frac{8\pi w\alpha}{3K})^{1/2} \tag{3.4}$$

where α is the contact radius and is given by

$$\alpha^3 = \frac{R}{K}[P + 3\pi wR + \sqrt{6\pi wRP + (3\pi wR)^2}] \tag{3.5}$$

For an applied load (P) of 10 nN the penetration depth was claculated to be 1 nm. Since the radius of the polymer globule is 10 nm the penetration is 10 %, which is small but not negligible and should be taken into account if the substrate is stiff. In order

to attain minimum deformation the applied force should be kept as low as possible and ideally negative and equal to the adhesive force.

3.4 Simple Geometric Deconvolution

In this study the polymer structures that will be investigated are expected to form spherical caps on the substrate with dimensions in the order of the tip's radius of curvature. If we consider a solid spherical cap on a flat substrate we can calculate its radius (r) contact angle (θ) and volume (V_c) in terms of its apparent half-width ($w_p = w/2$), height (h) and tip radius (R_t) by simple geometrical arguments [1] (fig. 3.7):

$$r = \frac{w_p^2}{2h} + \frac{h}{2} - R_t = \frac{w^2}{8h} + \frac{h}{2} - R_t \tag{3.6}$$

$$\cos\theta = 1 - \frac{h}{r} \tag{3.7}$$

$$V_c = \frac{1}{3}\pi r^3 (1 - cos\theta)^2 (2 + cos\theta) \tag{3.8}$$

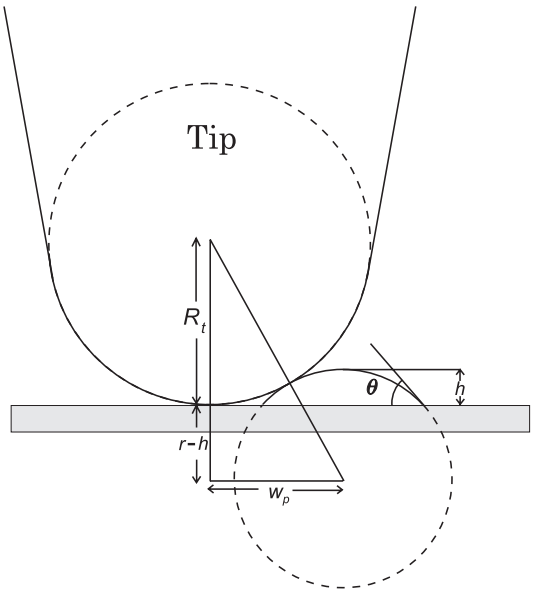

Figure 3.7: *Drawing showing a spherical cap of radius r forming a contact angle θ with the substrate scanned by a tip of radius R_t. h and w_p are the measured height and (apparent) halfwidth of the spherical cap respectively. When the substrate is flat, the height is measured correctly but the width is overestimated.*

[1] we assume that no deformation occurs

3.5 Measuring the Tip Radius

From the discussion above it is apparent that for obtaining true topographical information one should estimate the tip's radius of curvature. This can be attained by using edges of crystals. The edges of crystals appear rounded in the SFM images, because the image reflects the form of the tip rather than the crystal. Hence, the tip form and radius of curvature could be determined.

3.5.1 Experimental Part

Mica was cleaved in air and immediately placed in the vacuum chamber of a diffusion-pumped thermal evaporator (Edwards Auto 306). The mica sheets were heated to 400 ^{o}C at a pressure below 1x10^{-4} mbar. Gold was evaporated from resistively heated tungsten boats at a pressure below 5x10^{-6} mbar. The thickness of the gold layer was monitored with a quartz crystal oscillator and eventually amounted to 40 nm (deposition rate 3 nm/min). The gold substrates were left at 400 ^{o}C for 2 hours and then cooled down to room temperature in vacuum. The vacuum chamber was backfilled with prepurified nitrogen and the gold substrates were removed and stored under nitrogen until further use.

The scanning force microscopy experiments have been performed under water[2] Imaging was performed in the contact mode in the attractive regime (tip in contact with the surface and bent towards the surface) keeping the applied force constant (applied force $\approx$ adhesive forces). Commercially available and Si_3N_4 (V-shaped, force constants 0.032 N/m) cantilevers were used. The scanning speeds used were in the range of 5 μm/s.

3.5.2 Results and Discussion

In fig. 3.8a an image of the bare gold substrate is presented. Individual, atomically flat Au terraces separated by steps and deep channels (dark areas) can be observed. Zheng et. al. [23] have shown, using SEM at large incident angle (50^o), that the sides of the gold islands are sharp and nearly vertical. These channels' sides in SFM measurements look smoother and not at all vertical (see profile in fig. 3.8b) because of the finite tip radius of curvature (fig. 3.8c). From the triangle of fig. 3.8c we can deduce the tip radius:

$$R_t = \frac{w_m^2}{2h_m} + \frac{h_m}{2} \tag{3.9}$$

Here, w_m is the distance between the channel rim and the vertical tip radius and h_m the depth of the channel measured from the relevant channel rim. These quantities can be accurately measured from corresponding SFM line scans taken perpendicular to the channels.

[2]In ambient conditions, water condensation on the tip-apex creates meniscus forces that can act as an additional load. A remedy to this problem is to do the SFM experiments under water. Almost all measurements in this thesis have been performed in water.

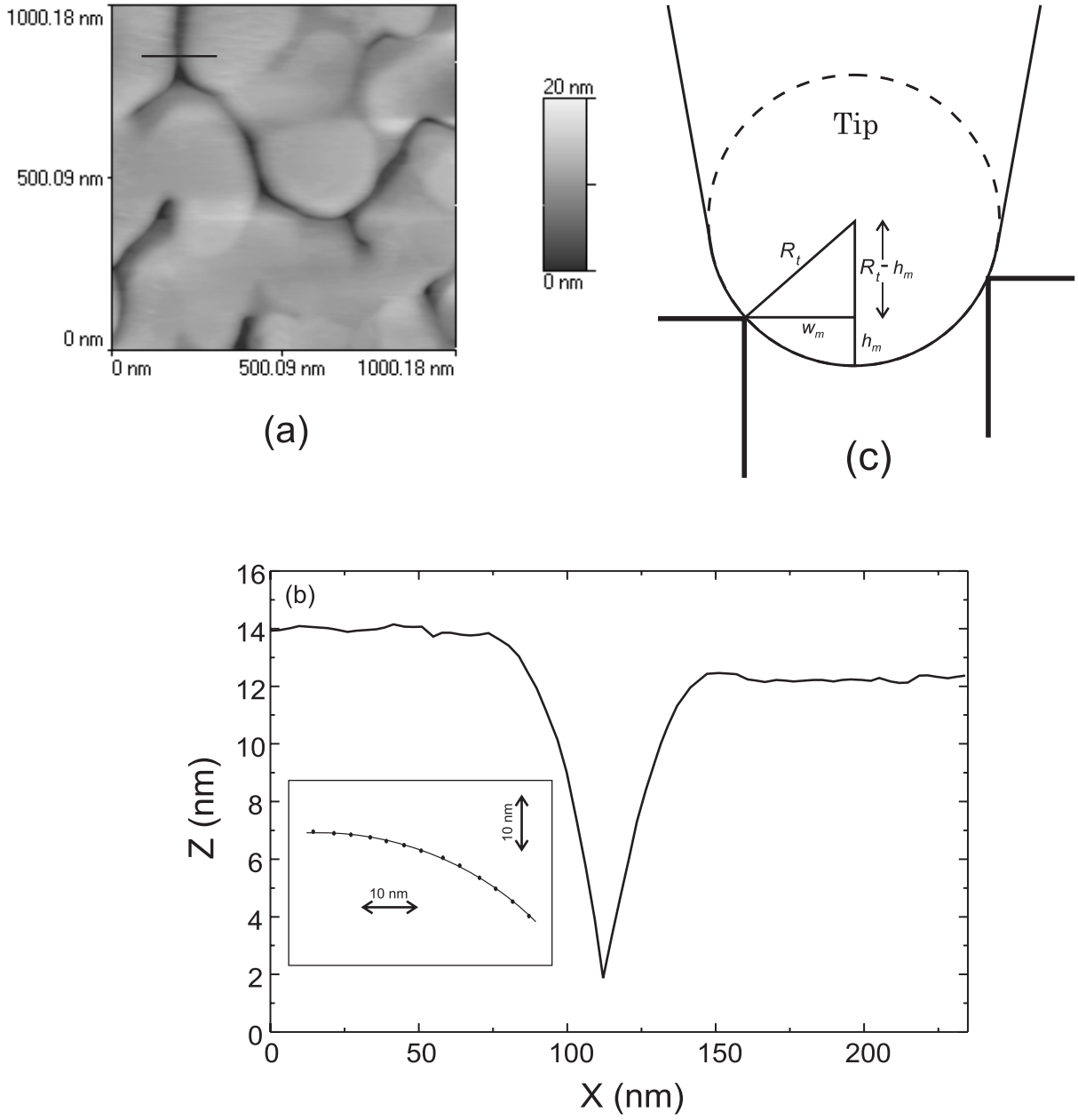

Figure 3.8: *(a) SFM topography image of the bare gold surface obtained by evaporation of 40 nm of gold onto a freshly cleaved mica substrate. The black line indicates the trace of the profile of a channel between gold islands as it is imaged by SFM and shown in (b). The insert figure shows the fitting of the SFM profile (black dots) of the island's edge with a circle of 55 nm radius. The edge, being very sharp, images the tip apex. (c) Drawing showing the imaging process of a channel between gold islands by an SFM tip. Due to the finite tip radius the depth of the channel is underestimated.*

A typical one is depicted in fig. 3.8. Care has to be taken that the width of the channel is smaller than the expected diameter of the tip. Using channels in various directions one can reconstruct the end of the tip quite accurately. In fact the *total* profile of the tip can be imaged as it is shown in the insert of fig. 3.8b. The black dots correspond to the measured profile of the channel's edge while the continuous line is a arc of a circle with radius of 55 nm. It is apparent that the channel's edge, being more acute than the tip, reveals its form.

Several tips' radii were measured (usually in four directions) using this procedure and the results were compared sucessfully with SEM pictures of the tips. The shapes of the tips were various from almost flat (at least in some directions) or rough to almost spherical like the one shown in the insert of fig. 3.8b. Generally their radius of curvature were around 50 nm in agreement with the manufacturer's claims.

3.6 Conclusions

We have demonstrated by simulations in the atomic scale and by experiments in the nanometer scale the generation of artefacts in SFM images due to the finite size of the tip. It was shown that in order to accurately measure the sizes of adsorbed particles, one should use flat substrates, apply low loads and measure independently the tip shape. An experimental method that reveals the form of the tip apex, based on imaging edges of gold crystals, has been described.

References

[1] Binnig, G.; Quate, C. F.; Gerber, Ch. *Phys. Rev. Lett.* **1986**, *56*, 930.

[2] Binnig, G.; Gerber, Ch.; Stoll, E.; Albrecht T. R.; Quate, C. F. *Europhys. Lett.* **1987**, *3*, 1281 ; *Surface Sci.* **1987**, *189-190*, 1.

[3] Whitman, L. J.; Stroscio, J. A; Dragoset, R. A.; Cellota, R. J. *J. Vac. Sci. Technol. B* **1991**, *9*, 770.

[4] Burnham, N. A.; Colton, R. J. *Scanning Tunneling Microscopy and Spectroscopy: Theory, Techniques and Applications* edited by Dawn A. Bonnell, VCH: New York, 1993.

[5] Oden, P. I.; Tao, N. J.; Lindsay, S. M. *J. Vac. Sci. Technol. B* **1993**, *11*, 137 .

[6] Landman, U.; Luedtke, W. D.; Ribarsky, M. W. *J. Vac. Sci. Technol. A* **1989**, *7*, 2829.

[7] Pethica, J. B. *Phys. Rev. Lett.* **1986** *57,* 3235.

[8] Abraham, F. F.; Batra, I. P. *Surf. Sci.* **1989**, *209* L-125.

[9] Colton, R. J.; Baker, S. M.; Driscoll, R. J., Youngquist M. J.; Baldeschwieler, J. D.; Kaiser, W. J.;*J. Vac. Sci. Technol. A* **1988**, *6*, 349.

[10] Mizes, H. A.; Park, S.-I.; Harrison, W. A. *Phys. Rev. B* **1987**, *36*, 4491.

[11] Fuchs, H.; Schimmel, Th.; Lux-Steiner, M.; Bucher, E. *Ultramicroscopy* **1992**, *42-44,* 1295.

[12] Ohnesorge, F.; Binnig, G. *Science* **1993**, **260**, 1451 (1993).

[13] Grutter, P.; Zimmermann-Edling, W.; Brodbeck, D.; *Appl. Phys. Lett.* **1992**, *60*, 2741.

[14] Burnham, N. A. *J. Vac. Sci. Technol. B* **1994**, *12(3)*, 2219.

[15] Hertz, H. *J. Reine Angew. Math.* **1881**, *92* 156.

[16] (a) Johnson, K. L.; Kendal, K.; Roberts, A. D. *Proc. R. Soc. Lond. A* **1971**, *324*, 301. (b) Sperling, G. Ph.D. Thesis in Karlsrule Technical High School, 1964.

[17] Derjaguin, B. V.; Muller, V. M.; Toporov, Yu. P. *J. Coll. Interf. Sci.* **1975**, *53*, 314.

[18] Maugis, D. *J. Coll. Interf. Sci.* **1992**, *150*, 243.

[19] *Handbook of Material Science*, edited by Charles T. Lynch, CRC Press: Cleveland, Ohio, 1975.

[20] Petersen, K. E. *Proc. IEEE* **1982**, *70*, 420.

[21] Sader, J. E.; Larson, I.; Mulvaney, P.; White, L. R. *Rev. Sci. Instrum.* **1995**, *66*, 3789.

[22] *Polymer Handbook*, third edition, edited by J. Brandrup and E. H. Immergut, Wiley: New York, 1989.

[23] Zheng, X.-Y.; Youzhen, D.; Bottomley, L. A. *J. Vac. Sci. Technol. B* **1995**, *13(3)*, 1320.